Carbon 203 (2023) 462–468

Contents lists available at ScienceDirect

Carbon

journal homepage: www.elsevier.com/locate/carbon

Research paper

# High-field and high-temperature magnetoresistance reveals the superconducting behavior of the stacking faults in multilayer graphene ☆

Christian E. Precker [a,1], José Barzola-Quiquia [a,2], Mun K. Chan [b], Marcelo Jaime [b], Pablo D. Esquinazi [a,*]

[a] Felix Bloch Institute for Solid-state Physics, University of Leipzig, Linnéstrasse 5, 04103, Leipzig, Germany
[b] National High Magnetic Field Laboratory, Los Alamos National Laboratory, Pulsed Field Facility, 87545, Los Alamos, NM, USA

ARTICLE INFO

*Keywords:*
Multilayer graphene
Defect-induced superconductivity
Stacking faults
Granular superconductivity
Magnetoresistance

ABSTRACT

In spite of 40 years of experimental studies and several theoretical proposals, an overall interpretation of the complex behavior of the magnetoresistance (MR) of multilayer graphene, i.e. graphite, at high fields ($B \lesssim 70$ T) and in a broad temperature range is still lacking. Part of the complexity is due to the contribution of stacking faults (SFs), which most of thick enough multilayer graphene samples have. We propose a procedure that allows us to extract the SF contribution to the MR we have measured at 0.48 K $\leq T \leq$ 250 K and 0 T $\leq B \lesssim$ 65 T. We found that the MR behavior of part of the SFs is similar to that of granular superconductors with a superconducting critical temperature $T_c \sim 350$ K, in agreement with recent publications. The measurements were done on a multilayer graphene TEM lamella, contacting the edges of the two-dimensional SFs.

## 1. Introduction

The recent discovery of superconductivity in twisted bilayer graphene [1,2], a stacking fault in itself, in trilayer graphene moiré superlattice [3] as well as in rhombohedral stacking order [4] at $T <$ 5 K supports the assumption that the origin of the "hidden superconductivity" reported in several bulk and mesoscopic graphite samples in the last 50 years [5–9], is related to the existence of two-dimensional stacking faults (SFs). Because these SFs are embedded in a multilayer-graphene matrix with a Bernal (2H) or rhombohedral (3R) stacking order, they can play a main role in the measured transport properties. Previous studies demonstrated that SFs, like twisted graphene layers, are common in well-ordered graphite samples [10–12]. Therefore, flat bands regions are expected to be found in bulk and mesoscopic graphite samples at certain SFs, where superconductivity at low and high temperatures is predicted [13–17]. Experimental evidence for the existence of a flat band has been reported for the 3R stacking order by scanning tunneling microscopy (STM) in Refs. [18–20] and by angle-resolved photoemission spectroscopy (ARPES) experiments near the $K$ point in Ref [21].

The tuning of superconductivity in mesoscopic bi- and trilayers graphene samples through the fabrication of regions with well-defined twist angle, added to the possibility of contacting directly the superconducting region, are clear advantages with respect to experimental studies in bulk or mesoscopic graphite samples. Although the existence of a large number of SFs can be recognized by Scanning Transmission Electron Microscopy (STEM) and X-rays Diffraction (XRD) analysis [22], the twist angle distribution remains largely unknown in thick multilayer graphene samples. However, there are some advantages in the study of the behavior of the SFs in well-ordered multilayer graphene or graphite samples. One of them is that SFs of very large areas (several 100's of $\mu m^2$) with high degree of lattice order can be found well shielded from environmental influence. Another advantage is that thick enough samples can have up to ~25% of the 3R stacking, in addition to the main 2H-type stacking [23,24]. The SFs between untwisted 2H and 3R crystalline regions are expected to have high superconducting temperatures [13–16]. This kind of SF has not yet been produced in a controllable way. On the other hand, if superconductivity is located at certain regions of such large SF areas, we expect to have

☆ The studies were partially supported by the DAAD Nr. 57207627, by the DFG under ES 86/29-1 and 31047526 (SFB 762) and the European Regional Development Fund Grant Nr.: 231301388. A portion of this work was performed at the National High Magnetic Field Laboratory, which is supported by the NSF Cooperative Agreement No. DMR-1644779, the US DOE and the State of Florida.

* Corresponding author.
*E-mail addresses:* christian.precker@aimen.es (C.E. Precker), esquin@physik.uni-leipzig.de (P.D. Esquinazi).
[1] Current address: AIMEN Technology Centre, Smart Systems and Smart Manufacturing-Artificial Intelligence and Data Analytics Laboratory, PI. Cataboi, 36418 Pontevedra, Spain.
[2] Current address: Goldschmidtstrasse 21, 04103 Leipzig, Germany.

https://doi.org/10.1016/j.carbon.2022.11.072
Received 7 September 2022; Received in revised form 15 November 2022; Accepted 24 November 2022
Available online 26 November 2022

granular and not homogeneous superconductivity, i.e. Josephson coupled superconducting regions of several tens of $\mu m^2$ each.

Which is the experimental evidence for the existence of superconductivity at certain SFs in multilayer graphene? For example, the results presented in Ref. [25] showed that contacting the edges of the SFs one is able to measure Josephson-like $I$–$V$ characteristics with a "zero" resistance range below a certain temperature-dependent critical current. The obtained critical temperatures, or the temperatures below which a percolation exists in a certain region of the tested SFs, depend on the prepared sample. In Ref. [26] a quantitative and qualitative comparison between one of the samples published in Ref. [25] and one of the bilayer twisted graphene published in Ref. [1] has been done. This comparison leaves no doubt about the origin of the observed superconductivity. Further experimental evidence of the last 20 years suggesting the SFs as the main origin for the superconducting as well as the metallic-like behavior of graphite samples are reviewed in Refs. [9,27,28]. Because the ideal graphite matrix is a narrow-gap semiconductor and the SFs not necessarily are at the near surface region of a macroscopic sample, a simple check of the influence of the SFs on the transport is to measure the resistance with electrodes at the top and at the edges. The obtained results in Refs. [29,30] show clearly the influence of the SFs on the transport properties. Double-wall carbon nanotubes can be taken as a material with some similarities to twisted bilayer graphene samples. It is therefore worth to note that double-wall carbon nanotubes can show superconductivity with critical temperatures ranging from ~3 K to ~20 K [31–33].

Our research covers the study of the low and very high field behavior of the magnetoresistance (MR) of the SFs in multilayer graphene extracted from the measured MR with the help of a procedure we developed. The results clarify several open questions on the interpretation of the MR of graphite and indicate the existence of superconducting regions with an upper critical temperature of ~350 K.

## 2. Methods and sample

We have prepared a multilayer graphene transmission electron microscope (TEM) lamella of dimensions 20 μm × 5 μm × 0.6 μm, with the width in the $c$-axis direction. The sample was prepared from a highly oriented pyrolytic graphite (HOPG grade A) bulk sample using a similar procedure as in [25], and investigated the transport properties at low- and high-fields (applied parallel to the $c$-axis) in a broad temperature range. The internal structure and the existence of SFs can be seen in the TEM images published for samples of the same batch in Refs. [28,34,35]. High resolution XRD results published in Ref. [36] revealed the existence of the 3R stacking order together with the main 2H phase.

The lamella was fixed on a substrate combining electron beam lithography with $SiN_x$ deposition covering part of the sample surface. Afterwards, the lamella was inductively etched with a plasma reactive ion etching system (ICP-RIE) to take out the disordered graphite layer formed during the milling process. Four electrodes were prepared with electron beam lithography and depositing Cr/Au, see the sample optical image in the inset of Fig. 2(b). The sample electrical resistance at 300 K was 7.44 Ω. As we show below, such a TEM lamella with the graphite $c$-axis parallel to the substrate provides the best way to get the SFs contribution to the total electrical resistance by contacting their edges. Considering the width (in the $c$-axis direction) of the sample and the corresponding STEM images in samples from the same batch, see Refs. [22,25], the number of SFs is significant. Therefore, our electrical voltage contacts pick up the response of several of them; the current input is distributed through all SFs. In this way, we expect to get the superconducting response of the SFs with the highest critical temperature.

For measurements at 2 K ≤ $T$ ≤ 300 K and DC magnetic fields $B \leq 7$ T we used a $^4$He cryostat, prior to the high field pulsed measurements. These last measurements were performed at the National High Magnetic Field Laboratory's Pulsed Field Facility (NHMFL-PFF) at Los Alamos National Laboratory (LANL) [37]. The measurements were done in a cryostat with a temperature range $T = 0.45$ K to 250 K, equipped with a 65 T multi-shot magnet, powered by a 32 mF, 4 MJ capacitor bank with a pulse duration of ~70 ms [38,39]. Most of the experiments were performed with pulses of 60 T. An alternating current of 12 μA amplitude was applied to the sample at a frequency of 50.5 kHz. The voltage was measured with a 20 MHz sampling rate. The field was always normal to the graphene planes and the SFs.

## 3. Results and discussion

Electrical transport measurements under high magnetic fields ($B >$ 10 T) performed in bulk and millimeter long multilayer graphene samples were reported in the last 40 years [40–43]. The observed behavior of the MR of those samples is complex and non-monotonous in field. Several interpretations were proposed, namely: fluctuations of charge density waves [44,45], magnetic freeze-out of carriers [46], 3D quantum Hall effect through the appearance of chiral surface states [42,47], the emergence of an excitonic BCS-like state [43], the appearance of an insulating surface states that carry no charge or spin within the planes [48], magnetic catalysis scenario [49–51], to cite a few of them. However, none of those studies considered the parallel contributions of at least two subsystems in graphite [35,52], i.e., the MR of the SFs and the one from the graphite matrix with mostly Bernal stacking order.

The incorrect interpretations of the transport, as well as the magnetization properties of graphite found in several early reports, relied on the assumption of electrically homogeneous samples. The lack of TEM or STEM characterization with the electron beam parallel to the graphene planes necessary to get an evidence of the existence of SFs, impeded in the past a timely development of the physics of graphite and of its SFs. One prominent example is the common, incorrect assumption that graphite is a semimetal with a finite Fermi surface at low temperatures. Systematic transport studies as a function of the thickness of graphite samples proved, however, that the SFs substantially contribute to the electrical transport and are at the origin of Shubnikov-de Haas (SdH) (or de Haas-van Alphen in the magnetization) quantum oscillations [30]. The vanishing of the SdH oscillations amplitude the smaller the thickness of the graphite samples, maintaining their high structural ordering, was recognized already at the beginning of 2000 without providing a clear interpretation of this behavior [53,54]. The change in the temperature and field dependence of the electrical transport as a function of the graphite sample thickness already indicated that the metallic like behavior vanishes when the thickness of the sample is smaller than the average distance between the SFs [34], which for the HOPG sample we used in this study means a length in the $c$-axis direction of less than ~30 nm. From different characterizations [19,35,52,55,56] we know nowadays that the intrinsic properties of *ideal graphite*, i.e. without SFs, are compatible with those of a narrow band semiconductor, not a semimetal and a finite Fermi surface does not exist at low temperatures. Stacking faults with superconducting behavior can be also found in mesoscopic and bulk samples, see [22] and Refs. therein.

The temperature dependence of the resistance at $B = 0$ is shown in Fig. 1(a). The resistance $R(T)$ increases with temperature to $T \simeq 165$ K, decreasing at higher $T$. This is one possible behavior of $R(T)$ for bulk and thick flakes of graphite reported in the literature [35,52]. The red line in Fig. 1(a) is a fit to a parallel resistance model given by the contribution of the SFs $R_i(T)$ and of the main ideal graphite matrix $R_{2H}(T)$ [35]:

$$\frac{1}{R(T)} \simeq \frac{1}{R_i(T)} + \frac{1}{R_{2H}(T)}, \tag{1}$$

where $R$ is the total sample resistance (see Refs. [35,52] for the full expression). $R_i(T)$ has an increasing with temperature contribution given by an exponential function of the form $R_i(T) \propto \exp(-E_a/k_B T)$.

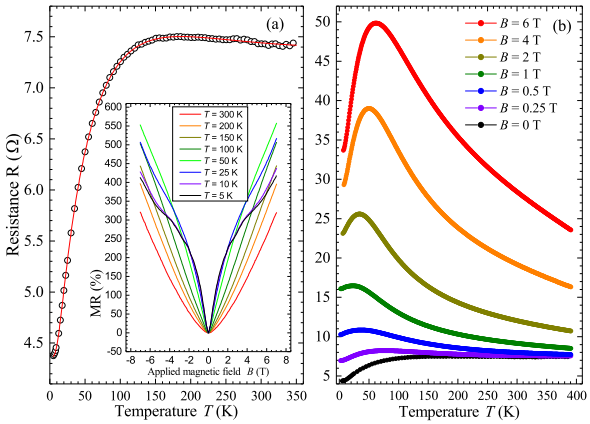


**Fig. 1.** (a) Temperature dependence of the electrical resistance of the TEM lamella at $B = 0$ T. The open circles represent the experimental data and the red line a fit to Eq. (1). The inset shows the MR at different constant temperatures at fields between $B \pm 7$ T. (b) Temperature dependence of the resistance at different magnetic fields.

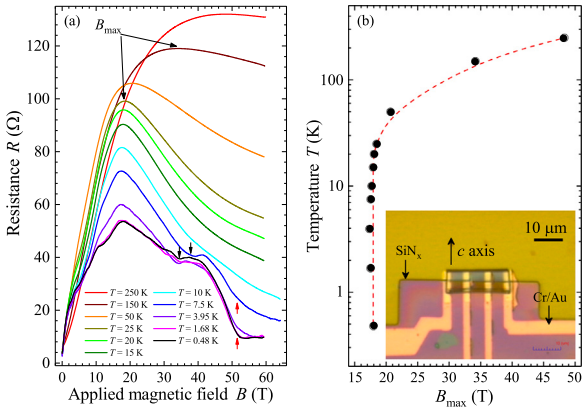


**Fig. 2.** (a) Pulsed magnetic field dependence of the resistance at different constant temperatures. The arrows point out the fields at the electronic phase transitions in graphite observed at $T < 10$ K. (b) Field $B_{max}$ where the MR has its maximum (see (a)) vs temperature. The red dashed line is a guide to the eye. The inset shows an optical image of the sample with its contacts and substrate.

The thermal activation energy $E_a \simeq 3$ meV is obtained from the fit. We note that this temperature dependent behavior is expected for granular superconductors according to Refs [57–60]. The value of the activation energy $E_a$ is similar to the one obtained from similar fits in eleven (11) graphite samples with different thickness [52]. The origin of this thermally activated behavior can be understood on the basis of the Langer–Ambegaokar–McCumber–Halperin (LAMH) model [58,59] for narrow superconducting channels in which thermal fluctuations can cause phase slips. The reason for the magnitude of the activation energy $E_a$, however, remains still open.

The narrow-gap semiconducting contribution of the 2H matrix can be approximated as $R_{2H}(T) \propto \exp(E_{g,2H}/(2k_BT))$ with an energy gap $E_{g,2H} \simeq 52$ meV obtained from the fit. All fit parameters are similar to those reported in the literature [35,52]. From measurements of the temperature dependence of the resistance of graphite samples with thickness between 35 nm and 6000 nm [52], the obtained values of the energy gap for the 2H and 3R stacking orders do not depend on the sample thickness within the given thickness range and experimental error. The parameters obtained from the fits shown in this work, emphasize that the measured sample is representative. Due to its small amount, we neglect the semiconducting parallel contribution of the 3R matrix to the total $R(T)$. We note that the excellent fits of $R(T)$ obtained for graphite samples of different thickness using the parallel resistance model and those exponential terms is not obtained by replacing them with $T^n$ or other dependencies found in the literature [52].

The inset in Fig. 1(a) shows the magnetoresistance defined as MR $= (R(B) - R(0))/R(0)$ measured at different constant temperatures with magnetic fields between ±7 T. At $T \leq 25$ K, SdH oscillations are detected with the main period in $B^{-1}$ of 0.21 $T^{-1}$ in agreement with the literature. From this period we estimate a 2D carrier density $n_{2D} \simeq 2.3 \times 10^{11}$ cm$^{-2}$ at certain SFs that originate the SdH oscillations [30]. Fig. 1(b) shows the $T$−dependence of the electrical resistance of the lamella at different magnetic fields. The sample shows the typical re-entrant metallic behavior at $B \gtrsim 1$ T and $T < 100$ K reported for bulk graphite samples [61].

Fig. 2(a) shows the absolute value of the electrical resistance of the lamella vs. magnetic field at different temperatures. The electronic transitions $\alpha$ (↓) and $\alpha'$ (↑) are clearly recognized at $T < 10$ K in the field range 30 T $< B <$ 55 T. Fig. 2(b) shows the $T$−dependence of the field $B_{max}$ at which the MR shows a maximum, see Fig. 2(a). We found that $B_{max}$ remains $T$−independent at $T \lesssim 25$ K. Above this temperature $B_{max}$ increases. This behavior is in very good agreement with that reported several times in the last 40 years [40,41,43,48,62,63]. In particular, the behavior of $B_{max}(T)$ was explained on the basis of the magnetic catalysis model [50]. From all the measured data we conclude that this TEM lamella shows all the characteristics of the electrical resistance and magnetoresistance of bulk graphite samples. We provide below an interpretation of the observed behavior.

We will extract first the SF resistance $R_i(T, B)$ from the measured $R(T, B)$ data. For that we rewrite Eq. (1) at a constant temperature as:

$$R_i(B) = R(B)/[1 - (R(B)/R_{2H}(B))]. \quad (2)$$

The MR of the 2H contribution can be described by the two-band model (TBM) appropriate for semiconductors and derived under the Boltzmann-Drude quasi-classical diffusive approach [23]. As emphasized above, the transport properties of ideal graphite (without SFs) match the ones of a narrow-band gap semiconductor. Therefore, we approximate the field-dependent resistance related to the semiconducting 2H-contribution as:

$$R_{2H}(B) \simeq R_{2H}(0) \cdot \left[ 1 + \frac{\mu^2 B^2 \left(1 - \frac{\Delta n^2}{n^2}\right)}{1 + \mu^2 B^2 \left(\frac{\Delta n^2}{n^2}\right)} \right], \quad (3)$$

where we have assumed equal mobility for both electrons and holes ($\mu = \mu_e \approx \mu_h$), and $\Delta n/n = (n_e - n_h)/(n_e + n_h)$ is the relative charge imbalance between electron $n_e$ and hole $n_h$ carrier densities.

The simplified expression of Eq. (3) has only two adjustable fitting parameters: the average mobility $\mu$ and the relative charge imbalance $\Delta n/n$; $R_{2H}(0)$ is a fixed parameter obtained from the fit in Fig. 1(a). Eq. (3) provides two key features of the MR of the semiconducting contribution, namely, the $B^2$ field dependence at low fields and its saturation at high enough fields.

Replacing Eq. (3) in Eq. (2), we obtain $R_i(B)$ plotted in Fig. 3(a). The results indicate that at $T < 25$ K, $R(B) \simeq R_i(B)$ because the semiconducting contribution becomes negligible, i.e. $(R_{2H}(B,T)/R(B,T))|_{T<25K} \gg 1$. We further note that $R_i(B)$ shows a maximum at $B'_{max} \simeq 18$ T, which does not depend significantly on $T$ within error, see Fig. 3(b). These results indicate that the temperature shift of $B_{max}(T)$ in the MR, see Fig. 2(b), is an artifact caused by the growing influence at $T > 25$ K of the semiconducting contribution $R_{2H}(B)$ in parallel to the SFs one. Regarding the parameters used, the charge imbalance between electrons and holes was assumed to be temperature and field independent $\Delta n/n = 0.05$. The only free parameter left is the mobility $\mu(T)$, which decreases with temperature (see inset in Fig. 3(b)). The temperature dependence of the mobility obtained from our fits is in qualitative agreement with the behavior found in the literature [64–66]. We note, however, that we neglect a ballistic contribution within

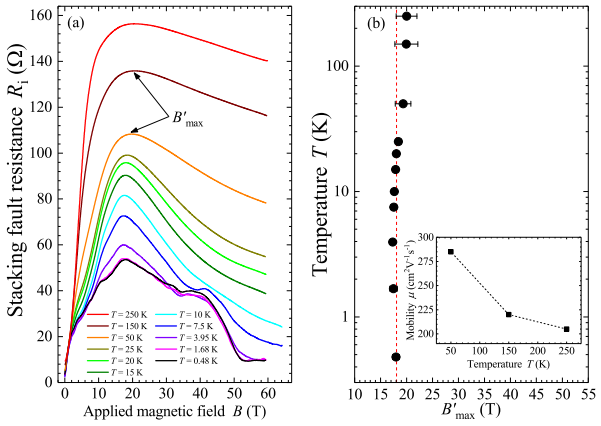


**Fig. 3.** (a) Field dependence of the SF resistance $R_i(B)$, calculated using Eq. (2), at different constant temperatures. (b) $B'_{max}$ vs temperature obtained from (a). The inset shows the temperature dependence of the carrier mobility.

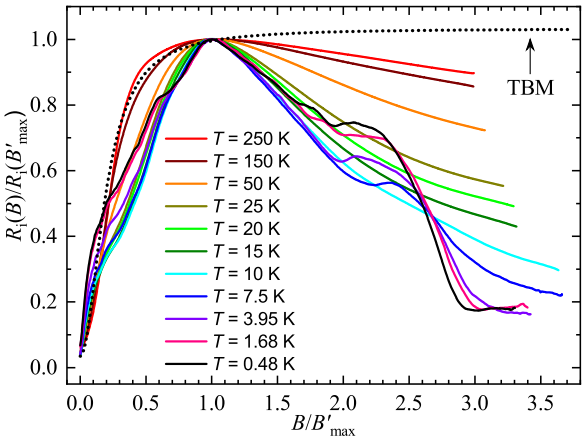


**Fig. 4.** Normalized SF contribution $R'_i$ vs normalized magnetic field at different constant temperatures. The dotted curve is the normalized MR obtained using the TBM, see Eq. (3).

the graphene layers of graphite, always present in micrometer large graphite samples [66]. It affects mainly the absolute value of the mobility obtained from the fitting to the diffusive part (Eq. (3)).

The MR of the SF ($R_i(B)$) plotted in Fig. 3(a), resembles the one observed in granular superconductors, like granular Al in a Ge matrix or InO films [67–69]. In particular, it shows a linear increase with field at low fields and decreases at fields above a certain field. The explanation for the linear increase with field discussed in the literature is based on the influence of the field in the Josephson coupling between superconducting regions or in our case 2D regions (or "grains") at some SFs. The higher the field, the larger is the number of uncoupled superconducting regions and the resistance increases linearly. After a maximum number of independent regions is reached at $B \sim B'_{max}$, a higher field increases the density of states inside those regions, increasing the probability of having Cooper pairs and the resistance starts to decrease with field. In this field range, the intragrain superconducting fluctuations affect the intergrain conductivity reducing the total resistance. This appears to be a general behavior in granular superconductors, see Fig. 7 in Ref. [56] and Refs. therein. We expect therefore that the field at which $R_i(B)$ starts to saturate can be considered as a critical field $B_{c2}$. This appears to be the case at a field $B \simeq B_{c2} \sim 50$ T $\sim 3B'_{max}$ at $T < 10$ K, see Fig. 3(a). However, we expect that $B_{c2}$ decreases with temperature, which is not clearly observed in $R_i(B)$ of Fig. 3(a) at $T \gtrsim 10$ K. The absence of a clear saturation at high temperatures and fields could be due to superconducting fluctuations, which in granular superconductors are expected to persist up to very high fields and temperatures [69].

Fig. 4 shows the normalized $R_i(B)$ vs the normalized magnetic field at different temperatures. We note that the higher the temperature the smaller is the decrease of the resistance with field at $B > B'_{max}$. This is expected because the number and/or size of the superconducting regions inside the SFs should in this case decrease. Therefore, at the highest critical temperature $T_c$ of the superconducting grains, there should not be a decrease with field of $R_i(B)$. At $T \geq T_c$ we expect a MR behavior similar to the semiconducting matrix, approximately given by the TBM, see Fig. 4.

Together with the similarities of our results to those of granular superconductors, let us emphasize here why we expect to have granular superconductivity at certain SFs and not a homogeneous state. Granular superconductivity occurs because the flat bands formed at the 2D SFs are not homogeneous in areas more than a few tens of micrometer square. This is obvious if we take into account the STEM evidence about the order or disorder that usual graphite samples have. Not only the perfection of a 2D SFs in the corresponding plane is an issue but also, e.g., the flat bands can be affected by the number of ideal graphene layers on both side of the interface. In addition, the graphene layers are not ideal over the sample, but have boundaries that restrict the homogeneous regions. This is a fact that is simple to recognize from STEM images taken at energies ~30 keV. The granular nature was already shown to be highly likely in several reports, as for example [25,70,71]. At low enough temperatures and currents in the nA region, $I$–$V$ curves indicate indeed a Josephson behavior and zero resistance within error [25]. Even the reported transition in twisted bilayer graphene mesoscopic samples does not appear to behave as a homogeneous but as a granular superconductor, as a direct, quantitative comparison between those results and the ones obtained in graphite TEM lamellae indicates [26].

The proposed interpretation of the MR of the SFs in terms of Josephson-coupled superconducting regions at certain interfaces or SFs, implies that at a fixed field the temperature dependence of the resistance should be compatible with the one expected for 2D granular superconductors. An analytical expression for the resistance of this 2D system within the effective medium approximation has been obtained in [60]. In particular, at fields near the critical field or at high enough temperatures the resistance between superconducting grains reaches a critical resistance $R_{JC}(T)$, which self-consistent solution (see Fig. 3 in [60]) follows nearly a $\ln(T/T_c)$ at $T/T_c > 0.2$, independently of the value of the assumed charging energy. We compare qualitatively this prediction with the difference between the normalized resistance in the normal state $R'_n$ and the normalized SF resistance ($R'_i = R_i(B)/R_i(B'_{max})$) from Fig. 4, $\Delta R = R'_n - R'_i$ at $B/B'_{max} = 2.8$ and 3. The difference $\Delta R$ follows a $\sim \ln(T/T_c)$ at high enough temperatures and a critical temperature $T_c = (351 \pm 20)$ K is obtained by extrapolation to $\Delta R = 0$, see Fig. 5. Interestingly, this $T_c$ agrees with the one suggested by different transport, magnetization [36,72,73] and magnetic force microscopy [74,75] measurements in different, well ordered natural graphite samples. At lower $T$, the behavior of $\Delta R(T)$ is affected by the transition to the normal state or by the electronic transitions, see Fig. 4, preventing a comparison with the predicted $R_{JC}(T)$ in the whole temperature range.

Temperature and field hysteresis of the magnetization at different applied magnetic fields and temperatures measured in similar HOPG samples, as the one used to prepare our TEM lamella, were published in Refs. [36,70], for example. In particular the difference vs. temperature between field cooled and zero-field cooled magnetic moment (where the huge diamagnetic background is automatically subtracted) indicates the existence of a similar critical temperature as the one obtained from the extrapolation in Fig. 5. The results in Ref. [70] show that a sample extracted from a HOPG sample with no or much lower density of SFs, shows no temperature and field hysteresis within experimental error, supporting the hypothesis that superconductivity is localized at the SFs.

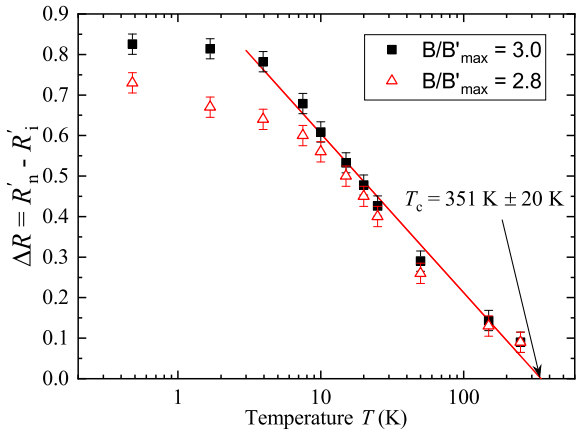


**Fig. 5.** Unitless difference between the normalized normal state and SF resistances at $B/B'_{max} = 3$ and 2.8 vs. temperature.

## 4. Conclusion

The MR of a multilayer graphene TEM lamella shows a temperature-dependent maximum at $B_{max}(T)$, which increases with temperature in agreement with earlier measurements of large graphite samples. Assuming that the MR is given by the parallel contribution of a semiconducting graphite matrix and of the stacking faults, we were able to extract the MR of this last in a broad temperature and magnetic field ranges. Our results indicate that the observed temperature dependence of $B_{max}(T)$ is an artifact due to the increasing contribution of the semiconducting graphite matrix with temperature. The extracted stacking fault MR shows several features compatible with those found in granular superconductors. The extrapolated maximum superconducting critical temperature of ~350 K for the superconducting regions at the stacking faults is in agreement with recent reports.

## Data availability

All the data included in the figures will be available at https://speicherwolke.uni-leipzig.de/index.php/s/X3TPRBwHYKrJM54 and on request from the corresponding author (PDE).

## CRediT authorship contribution statement

**Christian E. Precker:** Conception of the work, Data curation, Data analysis and interpretation, Writing – original draft. **José Barzola-Quiquia:** Conception of the work, Data curation, Data analysis and interpretation, Writing – review & editing. **Mun K. Chan:** Data curation, Writing – review & editing. **Marcelo Jaime:** Data curation, Writing – review & editing. **Pablo D. Esquinazi:** Conception of the work, Data analysis and interpretation, Writing – original draft.

## Declaration of competing interest

The authors declare that they have no known competing financial interests or personal relationships that could have appeared to influence the work reported in this paper.

## Acknowledgments

The authors thanks Zhipeng Zhang for the deposition of $SiN_x$, and Marius Grundmann for giving access the to ICP-RIE. C.E.P. gratefully acknowledges the support provided by the Brazilian National Council for the Improvement of Higher Education (CAPES) under 99999.013188/2013-05. MJ and MKC acknowledge support by the US DOE Basic Energy Science project "Science at 100T". All authors approved the final version of the manuscript.

## References

[1] Y. Cao, V. Fatemi, S. Fang, K. Watanabe, T. Taniguchi, E. Kaxiras, P. Jarillo-Herrero, Unconventional superconductivity in magic-angle graphene superlattices, Nature 556 (7699) (2018) 43–50, http://dx.doi.org/10.1038/nature26160.

[2] M. Yankowitz, S. Chen, H. Polshyn, Y. Zhang, K. Watanabe, T. Taniguchi, D. Graf, A.F. Young, C.R. Dean, Tuning superconductivity in twisted bilayer graphene, Science 363 (6431) (2019) 1059–1064, http://dx.doi.org/10.1126/science.aav1910.

[3] G. Chen, A.L. Sharpe, P. Gallagher, I.T. Rosen, E.J. Fox, L. Jiang, B. Lyu, H. Li, K. Watanabe, T. Taniguchi, J. Jung, Z. Shi, D. Goldhaber-Gordon, Y. Zhang, F. Wang, Signatures of tunable superconductivity in a trilayer graphene moiré superlattice, Nature 572 (2019) 215–219, http://dx.doi.org/10.1038/s41586-019-1393-y.

[4] H. Zhou, T. Xie, T. Taniguchi, K. Watanabe, A.F. Young, Superconductivity in rhombohedral trilayer graphene, Nature 598 (2021) 434–438, http://dx.doi.org/10.1038/s41586-021-03926-0.

[5] K. Antonowicz, Possible superconductivity at room temperature, Nature 247 (1974) 358–360, http://dx.doi.org/10.1038/247358a0.

[6] K. Antonowicz, The effect of microwaves on dc current in an Al-Carbon-Al sandwich, Phys. Stat. Sol. (A) 28 (1975) 497–502, http://dx.doi.org/10.1002/pssa.2210280214.

[7] Y. Kopelevich, P. Esquinazi, J. Torres, S. Moehlecke, Ferromagnetic- and superconducting-like behavior of graphite, J. Low Temp. Phys. 119 (2000) 691–702, http://dx.doi.org/10.1023/A:1004637814008.

[8] P. Esquinazi, N. García, J. Barzola-Quiquia, P. Rödiger, K. Schindler, J.-L. Yao, M. Ziese, Indications for intrinsic superconductivity in highly oriented pyrolytic graphite, Phys. Rev. B 78 (2008) 134516, http://dx.doi.org/10.1103/PhysRevB.78.134516.

[9] P. Esquinazi, Graphite and its hidden superconductivity, Pap. Phys. 5 (2013) 050007, http://dx.doi.org/10.4279/pip.050007.

[10] M. Kuwabara, D.R. Clarke, A.A. Smith, Anomalous superperiodicity in scanning tunnelling microscope images in graphite, Appl. Phys. Lett. 56 (1990) 2396, http://dx.doi.org/10.1063/1.102906.

[11] D.L. Miller, K.D. Kubista, G.M. Rutter, M. Ruan, W.A. de Heer, P.N. First, J.A. Stroscio, Structural analysis of multilayer graphene via atomic moiré interferometry, Phys. Rev. B 81 (2010) 125427, http://dx.doi.org/10.1103/PhysRevB.81.125427.

[12] M. Flores, E. Cisternas, J. Correa, P. Vargas, Moiré patterns on stm images of graphite induced by rotations of surface and subsurface layer, Chem. Phys. 423 (2013) 49–54, http://dx.doi.org/10.1016/j.chemphys.2013.06.022.

[13] N.B. Kopnin, M. Ijäs, A. Harju, T.T. Heikkilä, High-temperature surface superconductivity in rhombohedral graphite, Phys. Rev. B 87 (2013) 140503, http://dx.doi.org/10.1103/PhysRevB.87.140503.

[14] W.A. Muñoz, L. Covaci, F. Peeters, Tight-binding description of intrinsic superconducting correlations in multilayer graphene, Phys. Rev. B 87 (2013) 134509, http://dx.doi.org/10.1103/PhysRevB.87.134509.

[15] T. Heikkilä, G.E. Volovik, Flat Bands As a Route to High-Temperature Superconductivity in Graphite, Springer International Publishing AG Switzerland, 2016, pp. 123–144, http://dx.doi.org/10.1007/978-3-319-39355-1-6, Ch. 6,

[16] G.E. Volovik, Graphite, graphene, and the flat band superconductivity, JETP Lett. 107 (2018) 516–517, http://dx.doi.org/10.1134/S0021364018080052.

[17] T. Cea, N.R. Walet, F. Guinea, Twists and the electronic structure of graphitic materials, Nano Lett. 19 (12) (2019) 8683–8689, http://dx.doi.org/10.1021/acs.nanolett.9b03335.

[18] D. Pierucci, H. Sediri, M. Hajlaoui, J.-C. Girard, T. Brumme, M. Calandra, E. Velez-Fort, G. Patriarche, M.G. Silly, G. Ferro, V. Souliere, M. Marangolo, F. Sirotti, F. Mauri, A. Ouerghi, Evidence for flat bands near the Fermi level in epitaxial rhombohedral multilayer graphene, ACS Nano 9 (2015) 5432–5439, http://dx.doi.org/10.1021/acsnano.5b01239.

[19] R. Ariskina, M. Schnedler, P.D. Esquinazi, A. Champi, M. Stiller, W. Hergert, R.E. Dunin-Borkowski, P. Ebert, T. Venus, I. Estrela-Lopis, Influence of surface band bending on a narrow band gap semiconductor: Tunneling atomic force studies of graphite with bernal and rhombohedral stacking orders, Phys. Rev. Mater. 5 (2021) 044601, http://dx.doi.org/10.1103/PhysRevMaterials.5.044601.

[20] I. Hagymási, M.S.M. Isa, Z. Tajkov, K. Márity, L. Oroszlány, J. Koltai, A. Alassaf, P. Kun, K. Kandrai, A. Pálinkás, P. Vancsó, L. Tapasztó, P. Nemes-Incze, Observation.of. competing, Correlated ground states in the flat band of rhombohedral graphite, Sci. Adv. 8 (35) (2022) eabo6879, http://dx.doi.org/10.1126/sciadv.abo6879.

[21] H. Henck, J. Avila, Z. Ben Aziza, D. Pierucci, J. Baima, B. Pamuk, J. Chaste, D. Utt, M. Bartos, K. Nogajewski, B.A. Piot, M. Orlita, M. Potemski, M. Calandra, M.C. Asensio, F. Mauri, C. Faugeras, A. Ouerghi, Flat electronic bands in long sequences of rhombohedral-stacked graphene, Phys. Rev. B 97 (2018) 245421, http://dx.doi.org/10.1103/PhysRevB.97.245421.

[22] P.D. Esquinazi, C.E. Precker, M. Stiller, T.R.S. Cordeiro, J. Barzola-Quiquia, A. Setzer, W. Böhlmann, Evidence for room temperature superconductivity at graphite interfaces, Quantum Stud.: Math. Found. 5 (1) (2017) 41–53, http://dx.doi.org/10.1007/s40509-017-0131-0, arXiv:1709.00259.

[23] B.T. Kelly, Physics of Graphite, Applied Science Publishers, London, 1981.

[24] H. Wu, J. Song, S. Wang, J. Wen, A. Gu, Y. Dai, W. Li, H. Zhang, F.S. Boi, Coexistence of crystalline rhombohedral stacking and hexagonal moiré superlattices in exfoliated highly oriented pyrolytic graphite, Mater. Today Commun. (2022) 104152, http://dx.doi.org/10.1016/j.mtcomm.2022.104152.

[25] A. Ballestar, J. Barzola-Quiquia, T. Scheike, P. Esquinazi, Evidence of Josephson-coupled superconducting regions at the interfaces of highly oriented pyrolytic graphite, New J. Phys. 15 (2013) 023024, http://dx.doi.org/10.1088/1367-2630/15/2/023024.

[26] P.D. Esquinazi, Ordered defects: A roadmap towards room temperature superconductivity and magnetic order, 2019, http://dx.doi.org/10.48550/arXiv.1902.07489.

[27] P.D. Esquinazi, Y. Lysogorskiy, in: P. Esquinazi (Ed.), Basic Physics of Functionalized Graphite, in: Springer Series in Materials Science, vol. 244, Springer International Publishing AG Switzerland, 2016, pp. 145–179, http://dx.doi.org/10.1007/978-3-319-39355-1-7, Ch. 7.

[28] P.D. Esquinazi, C.E. Precker, M. Stiller, T.R.S. Cordeiro, J. Barzola-Quiquia, A. Setzer, W. Böhlmann, Evidence for room temperature superconductivity at graphite interfaces, Quantum Stud.: Math. Found. 5 (2018) 41–53, http://dx.doi.org/10.1007/s40509-017-0131-0.

[29] A. Hentrich, P.D. Esquinazi, Effects of the stacking faults on the electrical resistance of highly ordered graphite bulk samples, vol. c 6, no. 3, 2020, http://dx.doi.org/10.3390/c6030049.

[30] M. Zoraghi, J. Barzola-Quiquia, M. Stiller, P.D. Esquinazi, I. Estrela-Lopis, Influence of interfaces on the transport properties of graphite revealed by nanometer thickness reduction, Carbon 139 (2018) 1074–1084, http://dx.doi.org/10.1016/j.carbon.2018.07.070.

[31] W. Shi, Z. Wang, Q. Zhang, Y. Zheng, C. Ieong, M. He, R. Lortz, Y. Cai, N. Wang, T. Zhang, H. Zhang, Z. Tang, P. Sheng, H. Muramatsu, Y.A. Kim, M. Endo, P.T. Araujo, M.S. Dresselhaus, Superconductivity in bundles of double-wall carbon nanotubes, Sci. Rep. 2 (2012) 625, http://dx.doi.org/10.1038/srep00625.

[32] Y. Yang, G. Fedorov, J. Zhang, A. Tselev, S. Shafranjuk, P. Barbara, The search for superconductivity at van hove singularities in carbon nanotubes, Supercond. Sci. Technol. 25 (2012) 124005.

[33] J. Barzola-Quiquia, P. Esquinazi, M. Lindel, D. Spemann, M. Muallem, G. Nessim, Magnetic order and superconductivity observed in bundles of double-wall carbon nanotubes, Carbon 88 (2015) 16.

[34] J. Barzola-Quiquia, J.-L. Yao, P. Rödiger, K. Schindler, P. Esquinazi, Sample size effects on the transport properties of mesoscopic graphite samples, Phys. Stat. Sol. (A) 205 (2008) 2924–2933.

[35] N. García, P. Esquinazi, J. Barzola-Quiquia, S. Dusari, Evidence for semiconducting behavior with a narrow band gap of Bernal graphite, New J. Phys. 14 (5) (2012) 053015, http://dx.doi.org/10.1088/1367-2630/14/5/053015.

[36] C.E. Precker, P.D. Esquinazi, A. Champi, J. Barzola-Quiquia, M. Zoraghi, S. Muiños-Landin, A. Setzer, W. Böhlmann, D. Spemann, J. Meijer, T. Muenster, O. Baehre, G. Kloess, H. Beth, Identification of a possible superconducting transition above room temperature in natural graphite crystals, New J. Phys. 18 (2016) 113041, http://dx.doi.org/10.1088/1367-2630/18/11/113041.

[37] M. Jaime, A. Lacerda, Y. Takano, G.S. Boebinger, The national high magnetic field laboratory, J. Phys.: Conf. Ser. 51 (1) (2006) 643–646, http://dx.doi.org/10.1088/1742-6596/51/1/148.

[38] C. Swenson, W. Marshall, E. Miller, K. Pickard, A. Gavrilin, K. Han, H. Schneider-Muntau, Pulse magnet development program at NHMFL, IEEE Trans. Appil. Supercond. 14 (2) (2004) 1233–1236, http://dx.doi.org/10.1109/TASC.2004.830538.

[39] D.N. Nguyen, J. Michel, C.H. Mielke, Status and development of pulsed magnets at the NHMFL pulsed field facility, IEEE Trans. Appl. Supercond. 26 (4) (2016) 1–5, http://dx.doi.org/10.1109/TASC.2016.2515982.

[40] S. Tanuma, R. Inada, A. Furukawa, O. Takahashi, Y. Iye, Y. Onuki, Electrical properties of layered materials at high magnetic fields, in: S. Chikazumi, N. Miura (Eds.), Physics in High Magnetic Fields, first ed., in: 24 of Springer Series in Solid-State Sciences, Springer, Berlin, 1981, pp. 316–319, http://dx.doi.org/10.1007/978-3-642-81595-9.

[41] H. Yaguchi, J. Singleton, Destruction of the field-induced density-wave state in graphite by large magnetic fields, Phys. Rev. Lett. 81 (23) (1998) 5193–5196, http://dx.doi.org/10.1103/PhysRevLett.81.5193.

[42] B. Fauqué, D. LeBoeuf, B. Vignolle, M. Nardone, C. Proust, K. Behnia, Two phase transitions induced by a magnetic field in graphite, Phys. Rev. Lett. 110 (26) (2013) 266601, http://dx.doi.org/10.1103/PhysRevLett.110.266601, arXiv:1303.4074.

[43] K. Akiba, A. Miyake, H. Yaguchi, A. Matsuo, K. Kindo, M. Tokunaga, Possible excitonic phase of graphite in the quantum limit state, J. Phys. Soc. Japan 84 (5) (2015) 054709, http://dx.doi.org/10.7566/JPSJ.84.054709, arXiv:1503.04414.

[44] D. Yoshioka, H. Fukuyama, Electronic phase transition of graphite in a strong magnetic field, J. Phys. Soc. Japan 50 (3) (1981) 725–726, http://dx.doi.org/10.1143/JPSJ.50.725.

[45] G. Timp, P.D. Dresselhaus, T.C. Chieu, G. Dresselhaus, Y. Iye, Anomalous magnetoresistance of graphite at high magnetic fields, Phys. Rev. B 28 (12) (1983) 7393–7396, http://dx.doi.org/10.1103/PhysRevB.28.7393.

[46] N.B. Brandt, G.A. Kapustin, V.G. Karavaev, A.S. Kotosonov, E.A. Svistova, Investigation of the galvanomagnetic properties of graphite in magnetic fields up to 500 kOe at low temperatures, Sov. Phys.-JETP 40 (3) (1974) 564–569, http://jetp.ac.ru/cgi-bin/dn/e-040-03-0564.pdf.

[47] B.A. Bernevig, T.L. Hughes, S. Raghu, D.P. Arovas, Theory of the three-dimensional quantum hall effect in graphite, Phys. Rev. Lett. 99 (14) (2007) 5–8, http://dx.doi.org/10.1103/PhysRevLett.99.146804, arXiv:0701436.

[48] F. Arnold, A. Isidori, E. Kampert, B. Yager, M. Eschrig, J. Saunders, Charge density waves in graphite: Towards the magnetic ultraquantum limit, Phys. Rev. Lett. 119 (13) (2017) 136601, http://dx.doi.org/10.1103/PhysRevLett.119.136601.

[49] E. Gorbar, V. Gusynin, V. Miransky, I. Shovkovy, Magnetic field driven metal–insulator phase transition in planar systems, Phys. Rev. B 66 (2002) 045108, http://dx.doi.org/10.1103/PhysRevB.66.045108.

[50] D. Khveshchenko, Magnetic-field-induced insulating behavior in highly oriented pyrolitic graphite, Phys. Rev. Lett. 87 (2001) 206401, http://dx.doi.org/10.1103/PhysRevLett.87.206401.

[51] C. DeTar, C. Winterowd, S. Zafeiropoulos, Magnetic catalysis in graphene effective field theory, Phys. Rev. Lett. 117 (2016) 266802, http://dx.doi.org/10.1103/PhysRevLett.117.266802.

[52] M. Zoraghi, J. Barzola-Quiquia, M. Stiller, A. Setzer, P. Esquinazi, G. Kloess, T. Muenster, T. Lühmann, I. Estrela-Lopis, Influence of rhombohedral stacking order in the electrical resistance of bulk and mesoscopic graphite, Phys. Rev. B 95 (2017) 045308, http://dx.doi.org/10.1103/PhysRevB.95.045308.

[53] Y. Ohashi, T. Hironaka, T. Kubo, K. Shiiki, Magnetoresistance effect of thin films made of single graphite crystals, TANSO 195 (2000) 410–413.

[54] Y. Ohashi, K. Yamamoto, T. Kubo, Shubnikov - de haas effect of very thin graphite crystals, carbon'01, in: An International Conference on Carbon, Lexington, KY, United States, July 14-19, The American Carbon Society, 2001, pp. 568–570, available at www.acs.omnibooksonline.com.

[55] P. Esquinazi, J. Krüger, J. Barzola-Quiquia, R. Schönemann, T. Hermannsdörfer, N. García, On the low-field hall coefficient of graphite, AIP Adv. 4 (2014) 117121.

[56] J. Barzola-Quiquia, P.D. Esquinazi, C.E. Precker, M. Stiller, M. Zoraghi, T. Förster, T. Herrmannsdörfer, W.A. Coniglio, High-field magnetoresistance of graphite revised, Phys. Rev. Mater. 3 (5) (2019) 054603, http://dx.doi.org/10.1103/PhysRevMaterials.3.054603.

[57] Y. Shapira, G. Deutscher, Semiconductor-superconductor transition in granular al-ge, Phys. Rev. B 27 (1983) 4463–4466, http://dx.doi.org/10.1103/PhysRevB.27.4463.

[58] J.S. Langer, V. Ambegaokar, Intrinsic resistive transition in narrow superconducting channels, Phys. Rev. 164 (1967) 498–510, http://dx.doi.org/10.1103/PhysRev.164.498.

[59] D.E. McCumber, B.I. Halperin, Time scale of intrinsic resistive fluctuations in thin superconducting wires, Phys. Rev. B 1 (1970) 1054–1070, http://dx.doi.org/10.1103/PhysRevB.1.1054.

[60] Y.M. Strelniker, A. Frydman, H. Shlomo, Percolation model for the superconductor-insulator transition in granular films, Phys. Rev. B 76 (2007) 224528, http://dx.doi.org/10.1103/PhysRevB.76.224528.

[61] Y. Kopelevich, J.H.S. Torres, R.R. da Silva, F. Mrowka, H. Kempa, P. Esquinazi, Reentrant metallic behavior of graphite in the quantum limit, Phys. Rev. Lett. 90 (2003) 156402, http://dx.doi.org/10.1103/PhysRevLett.90.156402.

[62] Y. Iye, P.M. Tedrow, G. Timp, M. Shayegan, M.S. Dresselhaus, G. Dresselhaus, A. Furukawa, S. Tanuma, High-magnetic-field electronic phase transition in graphite observed by magnetoresistance anomaly, Phys. Rev. B 25 (8) (1982) 5478–5485, http://dx.doi.org/10.1103/PhysRevB.25.5478.

[63] H. Ochimizu, T. Takamasu, S. Takeyama, S. Sasaki, N. Miura, High-field phase in the magnetic-field-induced electronic phase transition of graphite, Phys. Rev. B 46 (4) (1992) 1986–1991, http://dx.doi.org/10.1103/PhysRevB.46.1986.

[64] C.A. Klein, W.D. Straub, Carrier densities and mobilities in pyrolytic graphite, Phys. Rev. 123 (1961) 1581–1583, http://dx.doi.org/10.1103/PhysRev.123.1581.

[65] L. Pendrys, C. Zeller, F. Vogel, Electrical transport properties of natural and synthetic graphite, J. Mater. Sci. 15 (1980) 12103–?2112, http://dx.doi.org/10.1007/BF00550638.

[66] P. Esquinazi, J. Barzola-Quiquia, S. Dusari, N. García, Length dependence of the resistance in graphite: Influence of ballistic transport, J. Appl. Phys. 111 (2012) 033709, http://dx.doi.org/10.1063/1.3682094.

[67] Y. Shapira, G. Deutscher, Semiconductor-superconductor transition in granular Al-Ge, Phys. Rev. B 27 (7) (1983) 4463–4466, http://dx.doi.org/10.1103/PhysRevB.27.4463.

[68] A. Gerber, A. Milner, G. Deutscher, M. Karpovsky, A. Gladkikh, Insulator-superconductor transition in 3D granular Al-Ge films, Phys. Rev. Lett. 78 (22) (1997) 4277–4280, http://dx.doi.org/10.1103/PhysRevLett.78.4277.

[69] V.F. Gantmakher, M.V. Golubkov, Giant negative magnetoresistance of semi-insulating amorphous indium oxide films in strong magnetic fields, JETP 82 (5) (1996) 951–958, http://www.jetp.ras.ru/cgi-bin/dn/e_082_05_0951.

[70] T. Scheike, P. Esquinazi, A. Setzer, W. Böhlmann, Granular superconductivity at room temperature in bulk highly oriented pyrolytic graphite samples, Carbon 59 (2013) 140–149, http://dx.doi.org/10.1016/j.carbon.2013.03.002.

[71] A. Ballestar, P. Esquinazi, W. Böhlmann, Granular superconductivity below 5 K in SPI – II pyrolytic graphite, Phys. Rev. B 91 (2015) 014502.

[72] S. Layek, M. Monteverde, G. Garbarino, M.-A. Méasson, A. Sulpice, N. Bendiab, P. Rodière, R. Cazali, A. Hadj-Azzem, V. Nassif, D. Bourgault, F. Gay, D. Dufeu, S. Pairis, J.-L. Hodeau, M. Núñez Regueiro, Possible high temperature superconducting transitions in disordered graphite obtained from room temperature de-intercalated $KC_8$, Carbon 201 (2023) 667–678, http://dx.doi.org/10.1016/j.carbon.2022.09.041.

[73] R. Rousset-Zenou, S. Layek, M. Monteverde, F. Gay, D. Dufeu, M. Núñez Regueiro, Hidden granular superconductivity above 500K in off-the-shelf graphite materials, 2022, https://arxiv.org/abs/2207.09149.

[74] M. Stiller, P.D. Esquinazi, J. Barzola-Quiquia, C.E. Precker, Local magnetic measurements of trapped flux through a permanent current path in graphite, J. Low Temp. Phys. 191 (2018) 105–121, http://dx.doi.org/10.1007/s10909-018-1859-6.

[75] R. Ariskina, M. Stiller, C.E. Precker, W. Böhlmann, P.D. Esquinazi, On the localization of persistent currents due to trapped magnetic flux at the stacking faults of graphite at room temperature, Materials 15 (2022) 3422, https://www.mdpi.com/1996-1944/15/10/3422.